Efficient computation of extended images by wavefield-based migration

Paul Sava, Center for Wave Phenomena, Colorado School of Mines and Ivan Vasconcelos, ION Geophysical*

SUMMARY

Extended common-image-point (CIP) gathers can be constructed using wave-equation migration by preserving into the output image the non-zero space- and time-lags of the cross-correlation between the source and receiver wavefields. Correct wavefield reconstruction leads to focused events in the extended CIPs, while incorrect reconstruction leads to de-focused events that can be used for velocity model building. This approach limits the number of locations where the multi-lag cross-correlation needs to be computed, thus reducing the computational cost of this method while preserving its capacity to indicate velocity errors. The cheaper cost is particularly important for wave-equation migration with wide-azimuth acquisition.

INTRODUCTION

Conventional seismic imaging methods share the assumption of single scattering at discontinuities in the subsurface. Under this assumption, waves propagate from seismic sources, interact with discontinuities and return to the surface as reflected seismic waves. We commonly discuss about a "source" wavefield, originating at the seismic source and propagating in the medium prior to any interaction with discontinuities, and a "receiver" wavefield, originating at discontinuities and propagating in the medium to the receivers (Berkhout, 1982). The two wavefields are kinematically equivalent at discontinuities. Any mismatch between the wavefields indicates inaccurate wavefield reconstruction typically assumed to be due to inaccurate velocity. In this context, we do not need to make assumptions about up- or down-going propagation, since waves can move in any direction as long as they scatter only once; we do not need to make any assumption about how we reconstruct those two wavefields as long as the wave-equation used accurately describes wave propagation in the medium under consideration.

We can formulate imaging as a process involving two steps: the wavefield reconstruction and the imaging condition. The key elements in this imaging procedure are the source and receiver wavefields, W_s and W_r. We can represent those wavefields as 4-dimensional objects, either in the time domain (for wavefield reconstruction using the two-way acoustic wave-equation) function of space $\mathbf{x} = \{x, y, z\}$ and time t, or in the frequency domain (for wavefield reconstruction using the one-way acoustic wave-equation) function of space and frequency ω. We need to analyze if the wavefields match kinematically and extract the reflectivity information using an imaging condition operating along the space and time axes. From the point of view of comparing the two wavefield objects, there is no intrinsic difference between space and time.

IMAGING CONDITIONS

A conventional cross-correlation imaging condition (cIC) based on the reconstructed wavefields can be formulated in the time or frequency domains (Claerbout, 1985):

$$R(\mathbf{x}) = \sum_{shots} \sum_{t} W_s(\mathbf{x}, t)\, W_r(\mathbf{x}, t) \tag{1}$$

$$= \sum_{shots} \sum_{\omega} \overline{W_s(\mathbf{x}, \omega)} W_r(\mathbf{x}, \omega)\,, \tag{2}$$

where R represents the migrated image and the over-line represents complex conjugation. This operation defines the image as the zero lag (in space and time) of the cross-correlation between the source and receiver wavefields. This property holds assuming that the wavefields are kinematically equivalent at discontinuities.

An extended cross-correlation imaging condition (eIC) (Rickett and Sava, 2002; Sava and Fomel, 2006) defines the image as a function of space and cross-correlation lags in space and time. This imaging condition can also be formulated in the time and frequency domains:

$$R(\mathbf{x}, \boldsymbol{\lambda}, \tau) = \sum_{shots} \sum_{t} W_s(\mathbf{x} - \boldsymbol{\lambda}, t - \tau)\, W_r(\mathbf{x} + \boldsymbol{\lambda}, t + \tau) \tag{3}$$

$$= \sum_{shots} \sum_{\omega} \overline{W_s(\mathbf{x} - \boldsymbol{\lambda}, \omega)} W_r(\mathbf{x} + \boldsymbol{\lambda}, \omega)\, e^{2i\omega\tau} \tag{4}$$

Equations 1-2 represents a special case of equations 3-4 for $\boldsymbol{\lambda} = 0$ and $\tau = 0$. The eIC defined by equations 3-4 can be used to analyze the accuracy of wavefield reconstruction. Assuming that all errors accumulated in the incorrectly-reconstructed wavefields are due to the velocity model, the extended images could be used for velocity model building using a tomographic approach (Sava and Biondi, 2004a,b). These extensions can also be converted to reflection angles (Sava and Fomel, 2003).

The main problem with the eIC is that it requires a large number of computations corresponding to the size of the image given by variable $\mathbf{x}$ and the number of space and time lags given by variables $\boldsymbol{\lambda}$ and τ. In practice, computing and saving the non-zero cross-correlation lags at all image coordinates is currently infeasible.

In order to analyze the cost of computing wave-equation images with extensions, we can rewrite the expression of the image obtained by eIC using the notation

$$R(x, y, z, \lambda_x, \lambda_y, \lambda_z, \tau)\ , \tag{5}$$

where x, y, z represent the space axes, and $\lambda_x, \lambda_y, \lambda_z$ represent space-lag extensions. We distinguish the following 4 special cases:

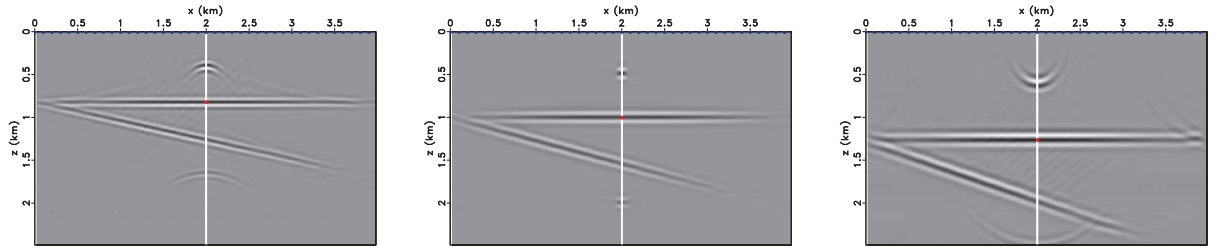

Figure 1: Synthetic model with images constructed using (a) slow velocity, (b) correct velocity and (c) fast velocity. The velocity error is 20% throughout the model. The CIP cubes depicted in Figures 2(a)-2(i) correspond to the diffractor and the horizontal and dipping reflectors at coordinates $z = \{0.50, 1.00, 1.50\}$ km when imaged with correct velocity.

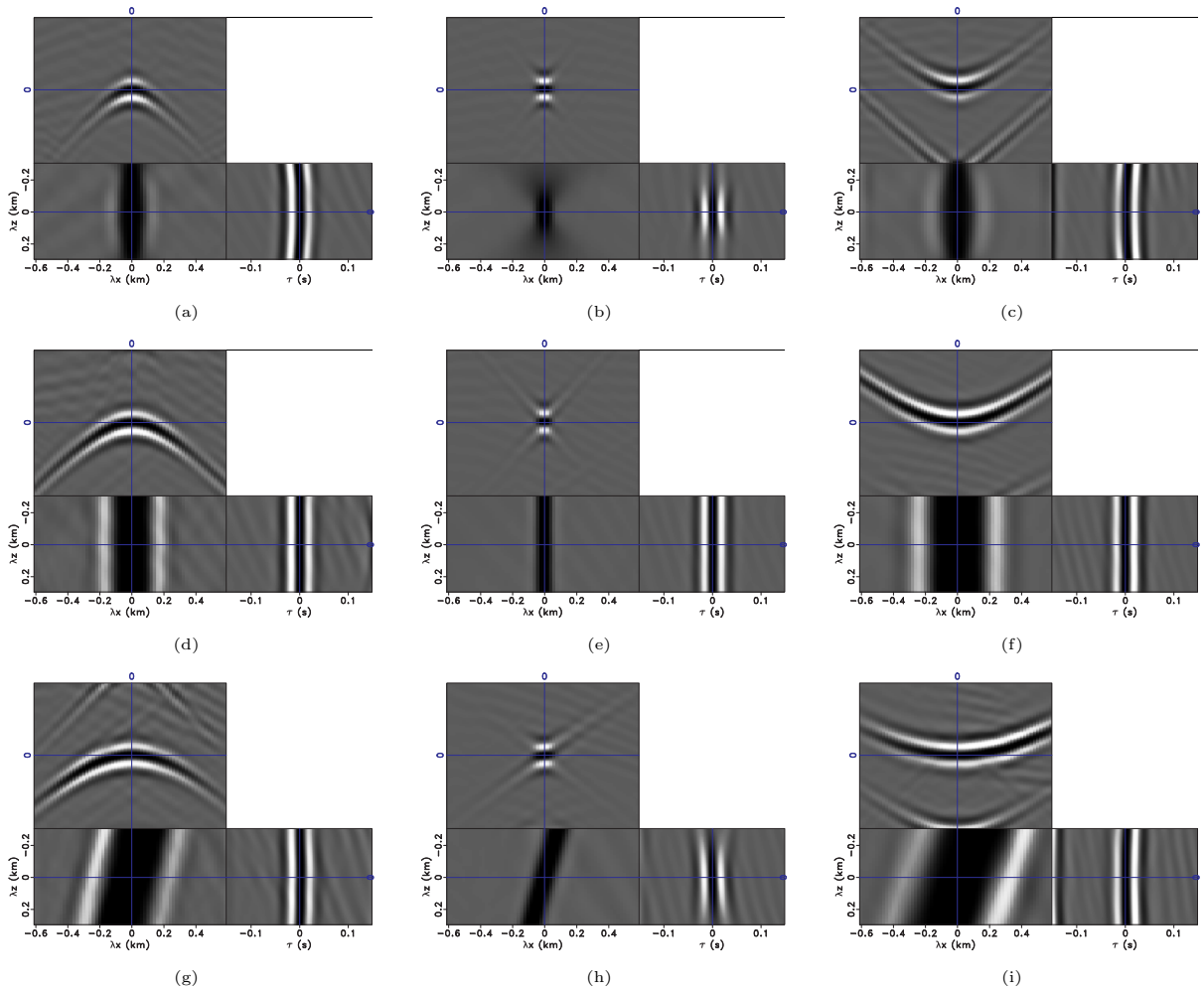

Figure 2: Extended common-image-point gathers corresponding to migration with slow velocity (panels a,d,g), correct velocity (panels b,e,h) and fast velocity (panels c,f,i). Panels (a,b,c) correspond to the diffractor, panels (c,d,e) correspond to the horizontal reflector and panels (g,h,i) correspond to the dipping reflector. The cubes depict CIPs function of space-lags λ_z, λ_x and time-lag τ. The slices shown intersect in the middle of the cubes, i.e. at zero cross-correlation lags. The value at zero lags represents the conventional image shown in Figures 1(a)-1(c).

1: imaging with no extensions
If we do not use any space extensions, the extended imaging condition reduces to cIC:

$$R\left(x,y,z,\lambda_x=0,\lambda_y=0,\lambda_z=0,\tau=0\right)\ . \qquad (6)$$

The computational cost C of cIC is proportional to the product $N_xN_yN_zN_\omega$, where N_x, N_y, N_z represent the number of samples along the space axes, and N_ω represents the number of frequencies used for imaging. We use this cost reference when we analyze other cases.

2: imaging with space-lag extensions
A common special case of wave-equation imaging with extensions is represented by images obtained with space-lag extensions only:

$$R\left(x=x_0,y=y_0,z,\lambda_x,\lambda_y,\lambda_z=0,\tau=0\right)\ . \qquad (7)$$

Assuming that we are computing the extensions at sparse space coordinates, we construct CIPs at $N=\frac{N_x}{\alpha_x}\frac{N_y}{\alpha_y}$ points, where α_i represent decimation coefficients, e.g. we compute the extensions at every α_x and α_y grid points in x and y. The computational cost of this type of imaging condition relative to the cost of cIC is

$$\frac{C_\lambda}{C}\sim\frac{N_{\lambda_x}N_{\lambda_y}}{\alpha_x\alpha_y}\ . \qquad (8)$$

If $N_{\lambda_i}=40$ and $\alpha_i=10$ $(i=\{x,y\})$, then $\frac{C_\lambda}{C}\sim 16$.

3: imaging with time-lag extension
Another common special case of wave-equation imaging with extensions is represented by images obtained with time-lag extensions only:

$$R\left(x=x_0,y=y_0,z,\lambda_x=0,\lambda_y=0,\lambda_z=0,\tau\right)\ . \qquad (9)$$

Assuming that we are computing the extensions at sparse space coordinates as in the preceding case, then the computational cost of this type of imaging condition relative to the cost of cIC is

$$\frac{C_\tau}{C}\sim\frac{N_\tau}{\alpha_x\alpha_y}\ . \qquad (10)$$

If $N_\tau=10^2$ and $\alpha_i=10$ $(i=\{x,y\})$, then $\frac{C_\tau}{C}\sim 1$, i.e. a much smaller cost than the one of imaging with space-lag extensions.

4: imaging with space- and time-lag extensions
A less common case of imaging with extensions is at the exact opposite end of the spectrum relative to cIC. Instead of computing images function of space coordinates, we can compute images function of extensions at fixed locations in the image (only one, in the limit):

$$R\left(x=x_0,y=y_0,z=z_0,\lambda_x,\lambda_y,\lambda_z,\tau\right)\ . \qquad (11)$$

We assume that we compute extensions at a finite number N of locations in the image. In this case, the total computational cost of this type of imaging condition is

$$\frac{C_{\lambda\tau}}{C}\sim N\frac{N_{\lambda_x}N_{\lambda_y}N_{\lambda_z}N_t}{N_xN_yN_z}\ . \qquad (12)$$

If $N_i=10^3$, $N_{\lambda_i}=40$ $(i=\{x,y\})$, $N_\tau=10^2$, and $N=10^3$, then $\frac{C_{\lambda\tau}}{C}\sim 5$, i.e. a cost smaller than the one of space-lag imaging, and comparable to the cost of time-lag imaging. We achieve smaller computational cost mainly because we can compute the image function of space-lag and time-lag extensions at a relatively small number of points distributed (non-uniformly) in the image, for example along the main reflectors identified in the image by a prior imaging with a cheaper imaging condition, e.g. cIC. This smaller computational cost is attractive for imaging if and only if the space- and time-lag extensions characterize properly the migrated images and, in particular, if they provide information about the velocity model accuracy.

COMMON-IMAGE-POINT GATHERS

The question we address in this section is whether the information provided by eIC at a single point characterizes the accuracy of wavefield reconstruction and is usable for velocity updates.

We can consider that the source and receiver wavefields in the immediate vicinity of a reflection point consist of plane waves. The space and time-lagged products of the source and receiver wavefields for one source position generate image planes containing zero space- and time-lag and with slopes depending on the local propagation direction. The superposition of those planes for all shots on the surface generates the CIPs shown in Figures 2(b)-2(e)-2(h). We observe focused events in the $\lambda_x-\tau$ panels indicating correct imaging. In contrast, if the source and receiver wavefields are reconstructed with incorrect velocity, then the superposition of the planes for all shots generates the CIPs line the ones shown in Figures 2(c)-2(f)-2(i) and Figures 2(a)-2(d)-2(g). We observe events with moveout in the $\lambda_x-\tau$ panel indicating incorrect imaging. As discussed in Vasconcelos et al. (2009), another interpretation of the extended imaging in this space is that they simply represent wavefields originating at the corresponding image point and propagating in its vicinity with the local medium parameters.

Consider the images depicted in Figures 1(a)-1(c) created by downward continuation from the same synthetic data using slow, correct and fast velocities. These images correspond to imaging without extensions, i.e. using cIC. The defocusing of sharp events (diffractors) indicate imaging inaccuracy which can be used for velocity model building (Sava et al., 2005; Fomel et al., 2007).

A similar analysis is possible for CIPs constructed with eIC. Figures 2(a)-2(b)-2(c), 2(d)-2(e)-2(f), and 2(g)-2(h)-2(i) correspond to the diffractor, the horizontal reflector and the dipping reflector, respectively. Figures 2(a)-2(d)-2(g), 2(b)-2(e)-2(h), and 2(c)-2(f)-2(i) correspond to imaging with slow, correct and fast velocities, respectively. We observe that if the velocity is correct, focusing occurs at zero lag in space and time. If the velocity is incorrect, focusing does not occur at zero space and time

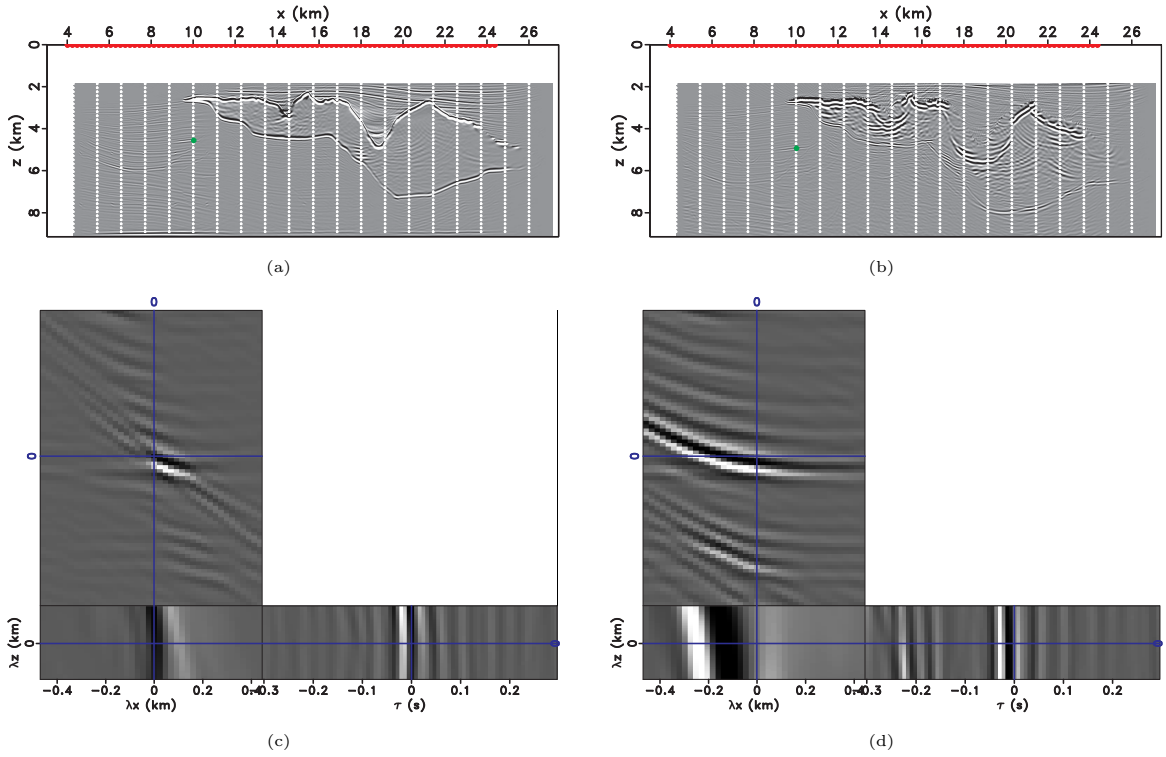

Figure 3: Sigsbee 2A migrated images using (a) correct and (b) fast velocities. The dots overlain on the image indicate the locations of extended CIPs. The dots on the surface indicate the locations of the shots used for imaging. Extended CIPs corresponding to (c) correct and (d) fast velocities. The events are truncated due to the off-end acquisition of surface data.

and the curvature of the events indicates the sign and magnitude of the velocity error. In all cases, an essential component of the CIPs is the time-lag axis which allows the analysis of focusing and defocusing indicating the accuracy of wavefield reconstruction. The analysis presented here is not possible without using the time-lag parameter. Furthermore, the vertical lag axis λ_z does not carry information for horizontal reflectors, but can potentially be used to evaluate structural dip, as can be seen by comparing Figures 2(e) and 2(h). Focusing in the lag domain allows for separation reflectors and diffractors, as seen by comparing Figures 2(b) and 2(e).

This analysis is applicable to more complex models, e.g. Sigsbee 2A (Paffenholz et al., 2002). Figures 3(a)-3(b) show migrated images using cIC. The dots overlain on the image indicate locations where extended CIPs are computed. Figures 3(c)-3(d) depict extended CIPs for a reflector located at coordinates $\{x, z\} = \{10.0, 4.5\}$ km in the image obtained with correct velocity. The CIPs correspond to imaging with correct (3(c)) and incorrect velocities (3(d)). As in the preceding example, the events are focused in the $\lambda_x - \tau$ panels when imaged with correct velocity, but de-focus when imaged with incorrect velocity. The events are partially truncated because of the off-end data acquisition.

CONCLUSIONS

Extended common-image-point gathers are effective tools for analyzing velocity accuracy for wave-equation imaging. The extended CIPs can be analyzed at sparse locations in the image volume, thus drastically reducing the computational cost of this method. One possibility is to construct extended CIPs along the main imaged reflectors which are the most indicative velocity model building components of migrated images. The sparse CIP computation also allows for easier visualization and interpretation of extended images.

A key requirement for the effectiveness of this technique is that space- and time-lag extensions be analyzed simultaneously. In addition to velocity analysis, potential applications include wide-azimuth angle-domain amplitude analysis, as well as slope estimation and separation of reflections and diffractions.

ACKNOWLEDGMENTS

Paul Sava acknowledges the support of the sponsors of the Center for Wave Phenomena at Colorado School of Mines. Ivan Vasconcelos acknowledges ION Geophysical for support of this research.